Dispersive-linear-chain approach to the interpretation of surface phonons: Application to GaSe(001) and $TaSe_2$(001)

L. Miglio
Dipartimento di Fisica dell'Università di Milano, Via Celoria 16, I-20133 Milano, Italy

L. Colombo
Dipartimento di Fisica "A. Volta" dell'Università di Pavia, Via Bassi 6, I-27100 Pavia, Italy
(Received 19 May 1987)

We outline a linear-chain model which is able to simulate fully the dynamics of a three-dimensional slab when some conditions are satisfied. This is achieved by allowing the force constants to have a dispersion which is fitted to neutron-scattering data. This procedure proves to be a useful tool for analyzing atom-scattering data of surface phonons in the framework of finite-chain calculations. Application to recent measurements in GaSe(001) and $TaSe_2$(001) is made, showing that, in spite of a common contrary opinion, relevant changes are required in the surface force constants to account for surface-phonon anomalies.

INTRODUCTION

Recent investigations on surface phonons in layered materials by He inelastic scattering[1,2] have proved that the dispersion of some surface modes is unexpectedly anomalous with respect to their bulk-band counterparts. These results seem to be in contrast with the general opinion that the formation of a surface by cutting weak Van der Waals interlayer forces should affect very slightly the dynamics of the atoms in the first layer.

A possible explanation for such a behavior may come from a detailed analysis of the electronic states at the surface. In particular, relevant changes in the charge distribution are able to modify in-plane and interplane force constants. However, as far as we know, there is no such information presently available for most layered compounds, so that a fully theoretical calculation of surface phonons is unattainable.

In this situation a phenomenological approach can be used to get some insight into which force constants are modified at the surface and how deep is the range of these changes. In particular a sufficiently simple model of a dispersive linear chain (DLC) can be fitted onto bulk phonons and then perturbed to reproduce surface modes. In this way not only is it possible to deduce if in-plane or interplane modifications have occurred, but also a correct surface-projected total phonon density is available for further applications.[3]

In the first section of this paper we discuss how to reproduce the exact dynamics of a bulk crystal through a linear chain approach. Then (Sec. II) we introduce a classification of surface perturbations and their effect on the slab-adapted dynamical matrix simulated by a finite linear chain. Finally (Sec. III) we discuss in this framework the experimental atom-scattering data of GaSe(001) and $TaSe_2$(001).

I. BULK DYNAMICS

For systems where two-dimensional periodicity is retained—such as slabs, semi-infinite crystals, or heterojunctions—the three-dimensional force constants can be Fourier transformed along the (x,y) plane which is parallel to the interface:

$$\phi_{\alpha\beta}(\mathbf{K}\mid l_3 l_3' ss') = \sum_{\mathbf{L}} \phi_{\alpha\beta}(\mathbf{L}\mid l_3 l_3' ss') e^{i\mathbf{K}\cdot\mathbf{R}(\mathbf{L})} , \quad (1)$$

where $(\mathbf{L},l_3)$ labels the slab-adapted unit cells[4] and $\mathbf{R}(\mathbf{L})$ specifies the points in the two-dimensional lattice of the surface. $\mathbf{K}$ is the wave vector lying in the (x,y) plane, s,s' and α,β are the atomic species and the Cartesian components, respectively.

The dynamical matrix satisfies the secular condition for the equation of motion

$$\sum_{l_3 s',\beta} D_{\alpha\beta}(\mathbf{K}\mid l_3 l_3' ss')\epsilon_\beta(\mathbf{K}j\mid l_3' s') = \omega_j^2(\mathbf{K})\epsilon_\alpha(\mathbf{K}j\mid l_3 s) \quad (2)$$

with

$$D_{\alpha\beta}(\mathbf{K}\mid ll_3' ss') = (M_s M_{s'})^{-1/2}\phi_{\alpha\beta}(\mathbf{K}\mid l_3 l_3' ss') , \quad (3)$$

and j assumes $N_3\times S\times 3$ values, N_3 being the number of cells along the z direction and S the number of atoms in the unit cell.

If the usual slab calculation is performed,[4] summation on the right side of Eq. (1) must be calculated for each $\mathbf{K}$. Moreover, for l_3 or l_3' belonging to the surface (interface) domain, perfect crystal force constants become perturbed ones, exploiting the symmetry breaking which occurs as the surface is created.

However if the force constants of the bulk are not available, nor the perturbation induced by the surface, a straightforward approach can be used. Suppose that each atom of the surface is a center of inversion with respect to its neighbors in the plane: the dynamical matrix of Eq. (2) is transformed into a real symmetric one[4] and the secular condition is formally (and therefore exactly) equivalent to that of a finite linear chain, which depends on $\mathbf{K}$ as a parameter. The summation on the right-hand side of Eq. (1) can be truncated to a reason-

 ©1988 The American Physical Society

able shell of values for $\mathbf{L}$, as long as Coulomb contributions are not dominant. By selecting a suitable set $\{\overline{\mathbf{K}}\}$ of points in the surface Brillouin Zone (SBZ), the coefficients $\phi_{\alpha\beta}(\mathbf{L}\,|\,l_3l_3',ss')$ of the expression (1) can be fitted onto $\phi_{\alpha\beta}(\overline{\mathbf{K}}\,|\,l_3l_3',ss')$. In order to determine the unperturbed set $\phi_{\alpha\beta}(\overline{\mathbf{K}}\,|\,l_3-l_3',ss')$ for the bulk, we must solve the implicit system of equations

$$\omega_j^2(\phi_{\alpha\beta}(\overline{\mathbf{K}}\,|\,K_z,ss'))=\omega_j^2(\overline{\mathbf{K}},K_z) \tag{4}$$

for each $\overline{\mathbf{K}}$, where the left side is calculated in a linear chain framework and the right one has been fitted to experimental dispersion curves.

In this way all nondiagonal terms $\phi_{\alpha\beta}(\mathbf{K}\,|\,l_3l_3',ss')$ can be obtained and the real symmetric matrix $D_{\alpha\beta}(\mathbf{K}\,|\,l_3l_3',ss')$ is constructed as a continuous function of $\mathbf{K}$. However there are still some points which ought to be discussed before treating the appearance of surface modes.

First, in a strictly linear chain model the diagonal elements of the force-constant matrix are determined by one-dimensional translational invariance (TI) conditions:

$$\phi_{\alpha\beta}^{\mathrm{LC}}(\mathbf{K}\,|\,l_3l_3,ss)=-\sum_{\substack{l_3,l_3',s,s'\\(l_3's')\neq(l_3s)}}\phi_{\alpha\beta}(\mathbf{K}\,|\,l_3l_3',ss') \tag{5}$$

(hereafter the superscript LC will label strictly linear chain diagonal elements). This constraint, valid for any value of the parameter $\mathbf{K}$, is too restrictive for the three-dimensional case. In fact, by applying TI to the real crystal we obtain

$$\begin{aligned}0&\equiv\sum_{l,s'}\phi_{\alpha\beta}(ls,ls')\\&=\sum_{\mathbf{K}}\left[\sum_{\mathbf{L}'}\frac{1}{N^2}e^{-i\mathbf{K}\cdot\mathbf{R}(\mathbf{L}')}\right]\sum_{l_3',s'}\phi_{\alpha\beta}(\mathbf{K}\,|\,l_3l_3',ss')\\&=\sum_{l_3',s'}\phi_{\alpha\beta}(\mathbf{K}=\mathbf{0}\,|\,l_3l_3',ss')\,,\end{aligned} \tag{6}$$

where N^2 is the number of surface unit cells in the Born–Von-Karman boundary conditions. As a consequence the term

$$d_{\alpha\beta}(\mathbf{K}\,|\,l_3s)\equiv\sum_{l_3',s'}\phi_{\alpha\beta}(\mathbf{K}\neq\mathbf{0}\,|\,l_3l_3',ss')\neq 0 \tag{7a}$$

must be added to the right side of expression (5) for a correct behavior of the long-wavelength acoustic modes.

The explicit form of $d_{\alpha\beta}(\mathbf{K}\,|\,l_3s)$ can be obtained by evaluating the difference

$$\begin{aligned}&\phi_{\alpha\beta}(\mathbf{K}\,|\,l_3l_3,ss)-\phi_{\alpha\beta}^{\mathrm{LC}}(\mathbf{K}\,|\,l_3l_3,ss)\\&\quad=\phi_{\alpha\beta}(\mathbf{L}=\mathbf{0}\,|\,l_3l_3,ss)+\sum_{\mathbf{L}\,(\neq\mathbf{0})}\phi_{\alpha\beta}(\mathbf{L}\,|\,l_3l_3,ss)e^{i\mathbf{K}\cdot\mathbf{R}(\mathbf{L})}\\&\qquad+\sum_{\substack{l_3',s'\\(l_3's')\neq(l_3s)}}\sum_{\mathbf{L}}\phi_{\alpha\beta}(\mathbf{L}\,|\,l_3l_3',ss')e^{i\mathbf{K}\cdot\mathbf{R}(\mathbf{L})}\,,\end{aligned} \tag{7b}$$

and by using the three-dimensional TI for the first term in (7b),

$$\begin{aligned}d_{\alpha\beta}(\mathbf{K}\,|\,l_3s)=&\sum_{\substack{\mathbf{L},l_3',s'\\(\mathbf{L},l_3',s')\neq(\mathbf{0},l_3,s)}}\phi_{\alpha\beta}(\mathbf{L}\,|\,l_3l_3',ss')\\&\times(e^{i\mathbf{K}\cdot\mathbf{R}(\mathbf{L})}-1)\end{aligned} \tag{8}$$

which becomes zero as $\mathbf{K}\to\mathbf{0}$, according to Eq. (6).

If we exploit the l_3 periodicity which is retained for bulk crystal, $\phi_{\alpha\beta}(\mathbf{K}\,|\,l_3-l_3',ss')$ has to be substituted in Eq. (8) so that $d_{\alpha\beta}(\mathbf{K}\,|\,s)$ will be equal for any layer in the infinite-chain case. This term can be fitted as an additional "diagonal force constant" to the neutron scattering experimental data. In particular this term incorporates the effects of the dynamics along the planes of atoms perpendicular to the linear chain.

When experimental bulk bands display little intermixing between different polarizations, which is usually the case for layered crystals, the DLC procedure can be applied separately for each of them. However, it may happen that the surface creation requires mixed components of the force constant matrix to be introduced. They can be taken into account *a posteriori* in the framework of a perturbative approach in the eigenvalue problem. In this case rotational invariance (RI) conditions are important to obtain $\phi_{\alpha\beta}(\mathbf{K}\,|\,l_3l_3',ss)'$ with $\alpha\neq\beta$. Moreover, they represent a way to account for the difference between strictly axial linear chains and "three-dimensional" linear chains (i.e., when not all the atoms lie on the same axis). In Appendix A we show how to take account of the RI condition in a DLC approach and how to obtain in a perturbative way the new eigenvalues of the mixed polarization system.

II. SURFACE PERTURBATIONS

We introduce now a set of different perturbations which produce the appearance of surface modes. Obviously they are not mutually excluding, but a qualitative analysis of experimental dispersion relation for surface phonons can indicate which is the dominant one.

The geometrical cut of interlayer forces that produces a slab formed by N_3 layers can be obtained by imposing new values $\tilde{\phi}_{\alpha\beta}=\phi_{\alpha\beta}+\Delta\phi_{\alpha\beta}$ on the force constants as follows:

$$\tilde{\phi}_{\alpha\beta}(\mathbf{K}\,|\,l_3\geq 1,\,l_3'<1,\,ss')=0\,, \tag{9a}$$

$$\tilde{\phi}_{\alpha\beta}(\mathbf{K}\,|\,l_3\leq N_3,\,l_3'>N_3,\,ss')=0\,, \tag{9b}$$

$$\Delta\phi_{\alpha\beta}(\mathbf{K}\mid l_3 l_3,ss)=\Delta\phi^{\mathrm{LC}}_{\alpha\beta}(\mathbf{K}\mid l_3 l_3,ss)+\Delta d_{\alpha\beta}(\mathbf{K}\mid l_3 s)$$
$$=-\sum_{\substack{l_3',s'\\(l_3's')\neq(l_3s)}}\Delta\phi_{\alpha\beta}(\mathbf{K}\mid l_3 l_3',ss')+\sum_{\substack{l_3',s'\\(l_3's')\neq(l_3s)}}\sum_{\mathbf{L}}\Delta\phi_{\alpha\beta}(\mathbf{L}\mid l_3 l_3',ss')(e^{i\mathbf{K}\cdot\mathbf{R}(\mathbf{L})}-1)$$
$$+\sum_{\mathbf{L}\,(\neq 0)}\Delta\phi_{\alpha\beta}(\mathbf{L}\mid l_3 l_3,ss)(e^{i\mathbf{K}\cdot\mathbf{R}(\mathbf{L})}-1)$$

$$=\sum_{s}\sum_{\substack{l_3'\\(l_3'>N_3,\,l_3'<1)}}\phi_{\alpha\beta}(\mathbf{K}=\mathbf{0}\mid l_3 l_3',ss')\ , \tag{9c}$$

where $1\le l_3\le N_3$ and we have assumed that no change for the in-plane force constants has occurred.

Conditions (9) do not provide relevant modifications of the phonon modes in layered crystals as the cut of Van der Waals forces correspond to a very weak perturbation. However, in other crystals, such as alkali halides, this perturbation turns out to be the leading one.

If a rigid relaxation of the first plane of atoms occurs to restore equilibrium conditions after the surface is created, in addition to the geometrical cut we have to change interplanar force constants in the first layer $l_3=l_3'=1,N_3$ as follows:

$$\Delta\phi_{\alpha\beta}(\mathbf{K}\mid l_3 l_3,ss')$$
$$=\sum_{\mathbf{L}}[P(ss')-1]\phi_{\alpha\beta}(\mathbf{L}\mid l_3 l_3,ss')e^{i\mathbf{K}\cdot\mathbf{R}(\mathbf{L})}$$
$$=[P(ss')-1]\phi_{\alpha\beta}(\mathbf{K}\mid l_3 l_3,ss') \tag{10a}$$

and

$$\Delta\phi_{\alpha\beta}(\mathbf{K}\mid l_3 l_3,ss)=\sum_{s'}[1-P(ss')]\phi_{\alpha\beta}(\mathbf{K}=\mathbf{0}\mid l_3 l_3,ss')\ , \tag{10b}$$

where P is a prefactor which describes either a stiffening ($P>1$) or a softening ($P<1$) of the interplane, short-range force constants.

This "rigid" perturbation does not affect qualitatively the dispersion of the surface modes created by the geometrical cut. In particular, it just produces a sensible gap between surface modes and bulk projected band edges, while the two dispersion laws remain quite similar as strong intralayer force constants have not been changed but only rescaled.

When the electronic charge rearrangements in the surface region modify the interactions between the atoms in the first layer, the dispersions along $\mathbf{K}$ for the DLC force constants are deeply affected. This is the most common situation in semiconductor surfaces where a reconstruction process may also occur; however this problem is out of the present analysis. In the case of first-sheet in-plane changes this contribution to the perturbation is restricted only to the diagonal elements:

$$\Delta\phi_{\alpha\beta}(\mathbf{K}\mid l_3 l_3,ss)\equiv\Delta d_{\alpha\beta}(\mathbf{K}\mid l_3 s)$$
$$=\sum_{\mathbf{L}\,(\neq 0)}\Delta\phi_{\alpha\beta}(\mathbf{L}\mid l_3 l_3,ss)\times(e^{i\mathbf{K}\cdot\mathbf{R}(\mathbf{L})}-1) \tag{11}$$

Modifications between atoms of different planes in the first layer are also possible so that this contribution must be added to the perturbation of Eq. (11) to obtain

$$\Delta\phi_{\alpha\beta}(\mathbf{K}\mid l_3 l_3,ss')=\sum_{\mathbf{L}}\Delta\phi_{\alpha\beta}(\mathbf{L}\mid l_3 l_3,ss')e^{i\mathbf{K}\cdot\mathbf{R}(\mathbf{L})} \tag{12a}$$

$$\Delta\phi_{\alpha\beta}(\mathbf{K}\mid l_3 l_3,ss)=-\sum_{\mathbf{L}}\sum_{\substack{l_3',s'\\(l_3's')\neq(l_3s)}}\Delta\phi_{\alpha\beta}(\mathbf{K}=\mathbf{0}\mid l_3 l_3',ss')$$
$$+\sum_{\mathbf{L}\,(\neq 0)}\Delta\phi_{\alpha\beta}(\mathbf{L}\mid l_3 l_3,ss)\times(e^{i\mathbf{K}\cdot\mathbf{R}(\mathbf{L})}-1) \tag{12b}$$

Equations (12) require a detailed knowledge of a surface force-constant changes, which can be evaluated only if electronic *ab initio* calculations are performed. In most of the cases, however, this information is not available and a good approach is to fit the new $\tilde{\phi}_{\alpha\beta}(\mathbf{K}\mid l_3 l_3',ss')$ to experimental surface phonons from atom scattering data along the borders of the irreducible SBZ. This procedure allows us to back transform to real space the DLC force constants for a physical interpretation to be performed. Obviously, this fitting has to be done by changing only a few force constants a time, to find out which are the most important ones. A preliminary distinction between in-plane and interplane changes is suggested.

III. APPLICATIONS TO GaSe(001) AND $TaSe_2$(001)

GaSe and $TaSe_2$ layered crystals are characterized by the sandwiching of a gallium dimer and a tantulum unit, respectively, between selenium atoms, forming a trigonal prismatic configuration. By applying two-dimensional periodicity this structure constitutes the layers of both crystals. Different ways of stacking these layers, which include plane displacements and rotations around the c

axis, give rise to several polytypes, such as ϵ-, β-, γ-, and δ-GaSe- and $2H_a$-, $4H_a$-, $4H_c$-, $3R$-, and $6R$-$TaSe_2$.[5] However, as long as no transition to another configuration takes place (such as to octahedral $TaSe_2$) the main dynamical features of these solids are rather independent of the stacking order. The unit cells of ϵ-GaSe and $2H_a$-$TaSe_2$ are shown in Figs. 1 and 2, respectively, along with their lattice parameters.

In Fig. 3 we display the structure of the (001) surface for both crystals, showing the surface unit cell and the SBZ. The two-dimensional Ga_2 (Ta) array of atoms is ordered in hexagonal network like the one of Se units. However, with respect to the Se units a rigid translation occurs so that the surface does not possess the inversion symmetry with respect to the c-axis that we required in Sec. I. Still, the very poor intermixing between x, y, and z components in the experimental dispersion curves on the basal plane[6-8] allows us to disregard this rigid translation and to consider a strictly axial linear chain for our model.

This ansatz not only puts us in the position to apply the DLC formalism for each Cartesian component separately, as a first-order approximation, but also makes the calculation suitable for any polytype. The *a posteriori* confirmation of our starting point comes from the very good fitting of surface-projected bulk dispersion relations

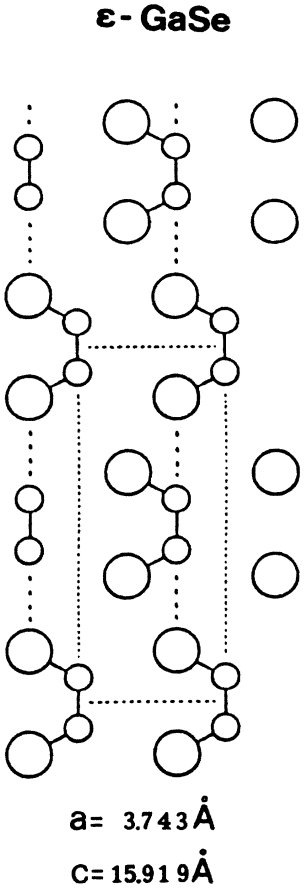

FIG. 1. Crystal structure of ϵ-GaSe. Unit cell and lattice parameters are displayed.

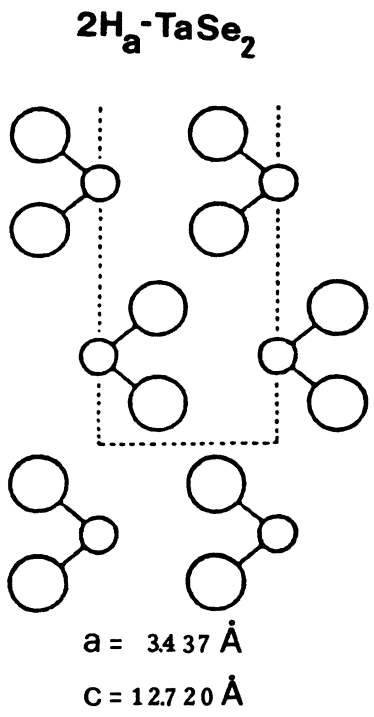

FIG. 2. The same as Fig. 1 for $2H_a$-$TaSe_2$.

that we have obtained.

In Appendix B are listed the $\{\mathbf{R}(\mathbf{L})\}$ vectors relative to four shells of neighboring cells in the (001) plane. If we truncate the summation in Eq. (1) to that set of $\{\mathbf{R}(\mathbf{L})\}$, we have to solve a linear system in thirty variables to fit $\alpha_{\alpha\beta}(\mathbf{L} \mid l_3 l_3', ss')$ onto $\phi_{\alpha\beta}(\bar{\mathbf{K}} \mid l_3 l_3', ss')$. This, in turn, would require a huge number of nonlinear systems to be solved in order to fit $\phi_{\alpha\beta}(\bar{\mathbf{K}} \mid l_3 l_3', ss')$ onto $\omega_j^2(\bar{\mathbf{K}}, K_z)$ according to Eq. (4). However, in a qualitative approach for nonionic materials, a much smaller range of interaction may be chosen. Moreover, if the set $\{\bar{\mathbf{K}}\}$ along the borders of the irreducible part of the SBZ has only an x or y component, an extensive grouping of

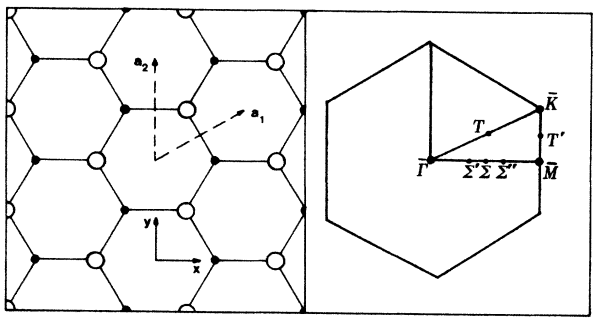

FIG. 3. Surface structure for (001) GaSe and $TaSe_2$. Two-dimensional unit vectors and the surface Brillouin zone are displayed.

$\phi_{\alpha\beta}(\mathbf{L} \mid l_3 l_3', ss')$ is allowed and the problem is greatly reduced. In Appendix C we show how to take into account this simplification for GaSe and $TaSe_2$ separately.

In Figs. 4(a) and 4(b) we display the dynamical model of the DLC that we have used for our calculations. $f_1(\mathbf{K})$ is the dispersive force constant that represents the covalent binding between a rigid dimer of Ga (or the Ta atom) and the Se shells; $f_3(\mathbf{K})$ stands for the electrostatic interaction between Se atoms, and $f_2(\mathbf{K})$ for the Van der Waals coupling between layers. g accounts for the electronic polarizability of Se atoms: In the $TaSe_2$ calculation we have set it equal to infinity (rigid-shell limit), since we have seen it play only a minor role in the GaSe case. The terms $d_{\alpha\beta}(\mathbf{K} \mid l_3 s)$, which are used as additional force constants to be fitted, here are labeled $d_1(\mathbf{K})$ and $d_2(\mathbf{K})$ [for Se atoms and Ga (Ta) atoms, respectively], since the l_3 dependence is present only near the surface.

Turning now to the problem of obtaining the relation between the frequency and the force constants [expression (4)], we derive from the equations of motion the eigenfrequencies of definite parity. First, we do this for the gerade vibration, characterized by the following values of the displacements coordinates:

$$\begin{aligned} u_2 &= 0 , \\ u_3 &= -u_1 , \\ v_3 &= -v_1 , \end{aligned} \tag{13}$$

where $u_{1,2,3}$ and $v_{1,3}$ stand for core and shell coordinates, respectively of Se (1,3) and Ga_2 or Ta (2). By using Eq. (13) we obtain

$$\omega_g^2 = \frac{1}{M_1}\left[\frac{f_1+2f_3+f_2[1+\cos(K_z a)]}{g+f_1+2f_3+f_2[1+\cos(K_z a]}g\right] - \frac{d_1}{M_1} , \tag{14}$$

where M_1 is the mass of Se atom, K_z is the wave vector along the chain and a is the lattice constant.

In the case of ungerade vibration, we have

$$\begin{aligned} u_2 &\neq 0 , \\ u_3 &= u_1 , \\ v_3 &= v_1 , \end{aligned} \tag{15}$$

In this symmetry, we obtain

$$\omega_u^2 = \frac{A}{2}+\frac{B}{2} \pm \left[\left[\frac{A}{2}-\frac{B}{2}\right]^2 + \frac{2f_1^2 g^2}{M_1 M_2 A_K^2}\right]^{1/2} , \tag{16}$$

where M_1 and M_2 are the Se and Ga_2 (Ta) masses, respectively, and

$$A = -\frac{d_2}{M_2}+\frac{2f_1}{M_2}\left[1-\frac{f_1}{A_K}\right] , \tag{17a}$$

$$B = -\frac{d_1}{M_1}+\frac{g}{M_1}\left[1-\frac{g}{A_K}\right] , \tag{17b}$$

$$A_K = f_1+g+f_2(1-\cos K_z a) . \tag{17c}$$

When the rigid shell limit ($g \to \infty$) is performed in Eq. (14) and (16), we have

$$\omega_g^2 = \frac{1}{M_1}[f_1+2f_3+f_2(\cos K_z a+1)-d_1] \tag{18}$$

and

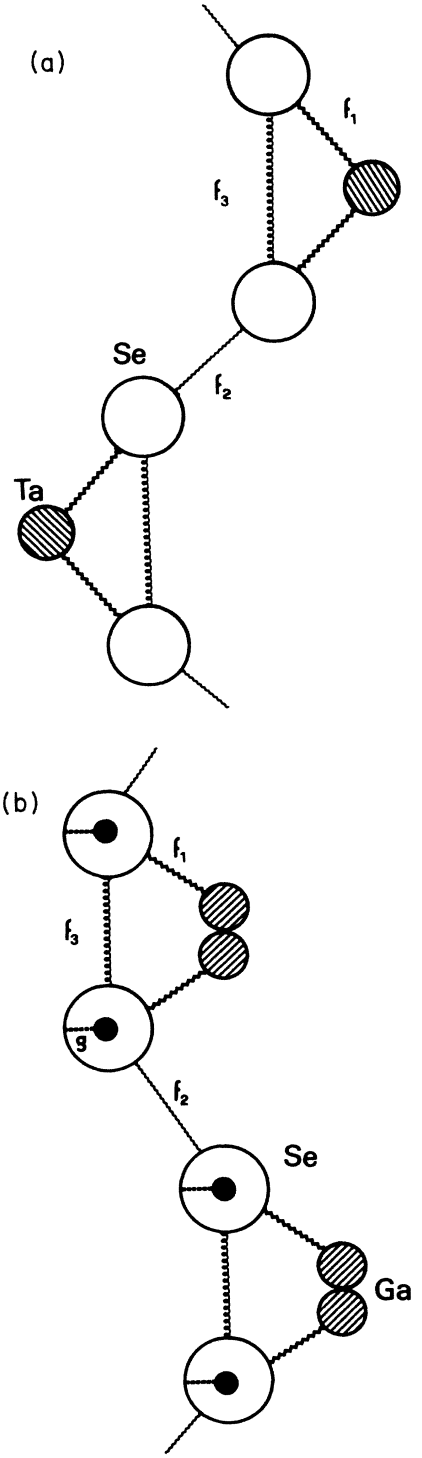

FIG. 4. Dynamical linear-chain models for $TaSe_2$ (a) and GaSe (b) used in the present calculations.

$$\omega_u^2 = \frac{A}{2} + \frac{B}{2} \pm \left[\left[\frac{A}{2} - \frac{B}{2} \right]^2 + \frac{2f_1^2}{M_1 M_2} \right]^{1/2} , \quad (19)$$

with

$$A = \frac{2f_1}{M_2} - \frac{d_2}{M_2} , \quad (20a)$$

$$B = \frac{f_1}{M_1} - \frac{f_2}{M_1}(\cos K_z a - 1) - \frac{d_1}{M_1} . \quad (20b)$$

Now, for each $\bar{\mathbf{K}}$ selected in the SBZ, Eqs. (14) and (16) or (18) and (19) for $K_z a = 0, \pi$ can be used to obtain $f_1(\bar{\mathbf{K}})$, $f_2(\bar{\mathbf{K}})$, $f_3(\bar{\mathbf{K}})$, $d_1(\bar{\mathbf{K}})$, and $d_2(\bar{\mathbf{K}})$ (g has a dispersionless large value). This step usually requires a numerical least-squares fitting procedure. However, some simplifications may be achieved by assuming a fixed value for some variables as a first-order approximation and improving the fitting subsequently. In the case of GaSe, for example, the ansatz $d_1(\mathbf{K})/M_1 = d_2(\mathbf{K})/M_2$ still allows a very good fit of projected bulk bands in the SBZ, while in the case of $TaSe_2$ we obtain a satisfactory description of the lattice dynamics even for dispersionless f_2 and f_3.

Appendix C shows how to use the set $f_1(\bar{\mathbf{K}})$, $f_2(\bar{\mathbf{K}})$, $f_3(\bar{\mathbf{K}})$, $d_1(\bar{\mathbf{K}})$, and $d_2(\bar{\mathbf{K}})$, fitted to experimental data of Refs. 7 and 8, to determine the dispersion law for each polarization.

In the following we will analyze separately the dispersion relations of surface phonons in GaSe(001) and $TaSe_2$(001). Figure 5 shows surface-projected bulk bands for x and z polarization (shaded areas) along the borders of the irreducible part of the SBZ for ϵ-GaSe(001). They are obtained with the force constants $f_{1\alpha\alpha}(\mathbf{K})$, $f_{2\alpha\alpha}(\mathbf{K})$, $f_{3\alpha\alpha}(\mathbf{K})$, and $d_{\alpha\alpha}(\mathbf{K})$ (where $\alpha = x$ or z) calculated according to Appendix C. Despite the fact that the DLC model is fitted only on a few points of the SBZ, a quite good agreement with the bulk dispersion curves of Jandl *et al.*[7] is found all over the zone. Obviously our calculation is not able to reproduce the eigenfrequencies of the Ga dimer, which is taken to be rigid, but their values lie much higher in the energy scale and are of little importance for the present analysis. Solid dots represent atom-scattering data for surface phonons and a detailed description of the experimental results can be found in Ref. 1. The labels S_n follow standard surface modes notation,[9] while E^i and A_n^i describe the optical character of bulk bands. By analysis of He scattering data we find that relevant anomalies are present all over the SBZ. Why are the surface optical branches farther from their respective bulk bands than the bandwidth? For the branch S_8 it is even difficult to determine which bulk band it comes from. The simplest interpretation could be based on what has been already observed on the (111) surface of noble metals: The S_8 mode is associated with the x-polarized E' acoustic band, and is greatly softened towards the zone boundary. At about $K = 0.8$ Å^{-1}, S_8 cuts the Rayleigh branch in both directions, so that we can interpret the soft branch in the TT' direction above 0.8 Å^{-1} as a continuation of the S_8 branch, rather than the conventional S_1 mode. According to this interpretation, S_8 has to be classified as an acoustic quasilongitudinal surface mode. Another interpretation of S_8 is based on the observation that it appears only at short wavelengths ($K > 0.4$ Å^{-1}), where S_2 starts to fade out, and disappears. We could imagine that S_2 is originally strongly softened in the zone-boundary region, down below the Rayleigh wave. However, such an anomalous dispersion curve cannot cross the pair of x bands (E'' and E') because of the intrinsic x-z coupling occurring at the surface, and therefore a large anticrossing behavior pushes apart the short- and long-wavelength sections of the S_2 branch. Of course, the supposed strong mixing with the E' band would finally give S_2 a strong x-polarized acoustic character, so that S_8 has more or less the same nature in both interpretations. In any case, it is clear that the observed dispersion curves imply large changes of force constants in the surface region. Such changes require, in turn, an extensive redistribution of the electron density, at the static and/or the dynamic level, in order to produce changes in bond strengths and polarizabilities.

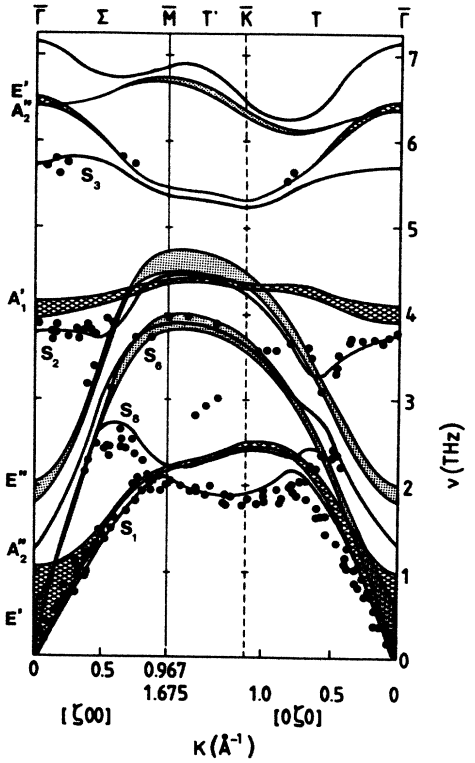

FIG. 5. Dispersion relations for bulk (shaded areas) and surface (solid lines) modes of ϵ-GaSe calculated along the borders of the Surface Brillouin Zone. Solid circles are experimental atom-scattering data from Ref. 1.

In our DLC model, geometrical cut and rigid relaxation of interplane force constants have proved not to induce any substantial change in the dispersion of surface modes with respect to the bulk bands. Nor is it possible to reproduce the experimental curves of Fig. 5. with a first-neighbor perturbation in the topmost sheet of Se atoms [$d_{\alpha\alpha}(\mathbf{K},1,1)$ fitting].

It turns out that the $f_{3zz}(\mathbf{K})$, which in the bulk is negative at the zone center and positive at the zone boundary, must be softened at the zone boundary to such an extent that it becomes strongly negative (attractive) everywhere. Moreover, a mixed isotropic contribution $f_{1xz}(\mathbf{K})$ must be added to that implied by the RI condition to take into account a new oblique Ga-Se interaction in the first layer. This term yields the mixing between x- and z-polarized modes at the surface, with the anticrossing mechanism mentioned above.

Quantitatively, if we get back to the leading coefficients of the Fourier expression

$$f(\mathbf{K})=f(\mathbf{L}^0)+f(\mathbf{L}^1)\cos[\mathbf{R}(\mathbf{L}^1)\cdot\mathbf{K}] +f(\mathbf{L}^2)\cos[\mathbf{R}(\mathbf{L}^2)\cdot\mathbf{K}]+\cdots ,$$

which corresponds to the force constants for the first shell of neighbors, we obtain the fitted bulk force constants and their change at the surface. Remembering that, according to Appendix C,

$$\Delta f_3(\mathbf{L}^1)/2\simeq\Delta f_3(\mathbf{L}^2)/4$$

represent the change in the Se-Se oblique intralayer interaction, while

$$\Delta f_1(\mathbf{L}^0)\simeq\Delta f_1(\mathbf{L}^1)\simeq\Delta f_1(\mathbf{L}^2)$$

is the Se-Ga perturbation, we have (in $\mathrm{kg\,s^{-2}}$)

$$f_{3zz}(\mathbf{L}^0)=+2.49,\quad \Delta f_{3zz}(\mathbf{L}^0)=+65.40 ,$$

$$f_{3zz}(\mathbf{L}^1)=-24.90,\quad \Delta f_{3zz}(\mathbf{L}^1)=+40.67 ,$$

$$f_{3zz}(\mathbf{L}^2)=-8.30,\quad \Delta f_{3zz}(\mathbf{L}^2)=+20.25 ,$$

$$f_{1zz}(\mathbf{L}^0)=+192.89 ,$$

$$\Delta f_{1xz}(\mathbf{L}^0)=\Delta f_{1xz}(\mathbf{L}^1)=\Delta f_{1xz}(\mathbf{L}^2)=41.37 ,$$

$$f_{1zz}(\mathbf{L}^0)=207.16 .$$

Calculated surface modes are shown in Fig. 5 (solid lines).

We note that the large softening of the Se-Se vertical interaction almost equals the stiffening of the total Se-Se oblique interaction, leading to a very modest relative softening of interplane force constant $f_{3zz}(\mathbf{K}=\mathbf{0})$. Moverover there is a negligible change of interactions with further neighbors in the layer and an appreciable growth of the nearest-neighbor Se-Se nondiagonal force constant f_{1xz}; this change, however, is a small quantity compared to diagonal force constants f_{1xx} or f_{1zz}.

The softening of the vertical Se-Se radial interaction, the stiffening of the oblique interactions between Se ions in adjacent cells (passing through the Se-Ga xz force constant) suggest, altogether, a complex modification of the bond-charge distribution within the surface layer. Strictly speaking, it is the susceptibility of bonding electrons with respect to lattice vibrations that is to be changed: Thus, the existence of localized excited states at the surface would be required. Recent inverse-photoemission experiments and band-structure calculations have proved that localized excited surface states do occur even in a layered crystal as weakly bound as graphite.[10] Since also in GaSe there is much electronic change between the layers in the excited states,[11] we expect surface excited states in the crystal as well.

We turn now to the case of $2H$-$TaSe_2$. A charge density wave (CDW) instability at 122.2 K is found which maintains the incommensurate superstructure down to 90 K.[5] The electron-phonon coupling driving the CWD behavior is also responsible for the appearance of strong phonon anomalies in the longitudinal acoustic (LA) bulk dispersion curve at a wave vector equal to $2k_f$: neutron scattering data by Moncton[8] are available for the lower part of the phonon spectrum. On this basis, a model calculation has been performed by Feldman[6] which agrees quite well with experimental data for acoustic phonons and which reproduces the dramatic softening of the longitudinal mode driven by the CDW. However, high-frequency optical modes can be compared only to Raman measurements at the $\bar{\Gamma}$ point[8,12] and their dispersion cannot be confirmed by neutron scattering data. Although atom-scattering information is presently available, mostly for the Rayleigh wave (RW) along the $\bar{\Gamma}$-$\bar{M}$ direction, some points are detected also for surface optical phonons, so that within the hypothesis that no surface perturbation affects this frequency region they can be used to fix an experimental frame for bulk band dispersion. Anyway, our analysis will be confined to understanding the behavior of the RW with respect to the transverse acoustical (TA) bulk band edge.

Figure 6 displays, along the $\langle 100\rangle$ direction, surface-projected bulk modes (shaded areas) for nearly-x and nearly-y polarization, as deduced from a fitting of the DLC model on neutron scattering data,[5] atom scattering data,[2] and Raman measurements.[12] $T=140$ K experimental He-scattering measurements are represented by black circles.[2] A strongly localized Rayleigh mode branch is found for two different surface temperatures above and below the CDW transition.[2] Furthermore, the Rayleigh branch is found to have an anomaly at approximately one-half of the $\bar{\Gamma}\bar{M}$ direction. Such an anomaly appears to be displaced with respect to the LA bulk anomaly (occurring at about two-thirds of that direction), but shows a similar temperature-dependent softening. A careful study of the temperature dependence of the anomaly will be presented elsewhere. Here we want to point out only that a remarkable gap appears at the zone boundary between the bulk band edge and the RW.

A good fit for the bulk experimental (neutron and He) data for z polarization is obtained with the following interplanar and intraplanar force constants (all in units of $\mathrm{kg\,s^{-2}}$)

$$f_{1zz}(\mathbf{K})=20.91+3.42\cos[\mathbf{R}(L^1)\mathbf{K}] ,$$

$$f_{2zz}(\mathbf{K})=0.895 ,$$

$$f_{3zz}(\mathbf{K})=-0.089 ,$$

$$d_{1zz}(\mathbf{K})=4.30\{1-\cos[\mathbf{R}(L^1)\mathbf{K}]\} ,$$

$$d_{2zz}(\mathbf{K})=0.94\{1-\cos[\mathbf{R}(L^1)\mathbf{K}]\} .$$

In the fitting procedure the dispersion of the weak force constants f_2 and f_3 has been neglected. Actually the in-

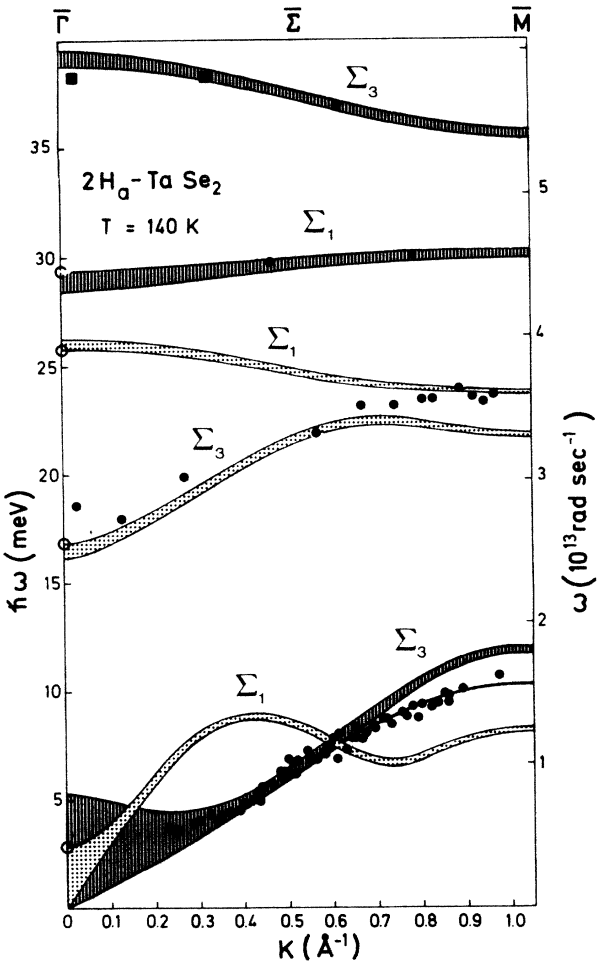

FIG. 6. Dispersion relations for bulk (shaded areas) and surface (solid line) modes of $2H_a$-$TaSe_2$, calculated along the $\bar{\Gamma}\bar{M}$ direction. Dotted bands display nearly-x polarization and the other ones have nearly-z displacements. Solid circles ($T=140$ K) and solid squares ($T=60$ K) represent experimental atom-scattering data from Ref. 2.

teraction between the two Se sheets within the layer is very weak and slightly attractive, presumably because of the large screening of the Ta sheet with its free electrons.

In order to fit the Rayleigh wave dispersion (instead of edge of the bulk TA branch) different values of f_{1zz}, the intraplanar force constants, are required:

$$f^s_{1zz}(\mathbf{K})=21.07+3.26\cos[\mathbf{R}(L^1)\mathbf{K}] ,$$

$$d^s_{1zz}(\mathbf{K})=4.15\{1-\cos[\mathbf{R}(L^1)\mathbf{K}]\} ,$$

$$d^s_{2zz}(\mathbf{K})=-0.30\{1-\cos[\mathbf{R}(L^1)\mathbf{K}]\} .$$

Thus the surface perturbation amounts to

$$\Delta d_{1zz}(\mathbf{K})=-\Delta f_{1zz}(\mathbf{K})=-0.16\{1-\cos[\mathbf{R}(L^1)\mathbf{K}]\} ,$$

$$\Delta d_{2zz}(\mathbf{K})=-1.25\{1-\cos[\mathbf{R}(L^1)\mathbf{K}]\} .$$

We see that most of the surface perturbation, which yields a softening of the Rayleigh wave at the zone boundary, is concentrated in the Ta sheet. Here an appreciable attraction is switched on at the surface, which gives a negative d^s_{2zz}. This is consistent with the occurrence of a charge density wave instability in the gas of conduction electrons provided by the tantalum sheet. A similar situation is found in the fitting of the x-polarized dispersion curves, even if we do not consider surface modes in this case. The presence of the anomaly in the bulk LA dispersion curve implies at least three Fourier components in the representation of the bulk modes. Those depicted by shaded areas in Fig. 6 are based on the fit (in kg s^{-2}):

$$f_{1xx}(\mathbf{K})=7.03+3.10\cos[\mathbf{R}(L^1)\mathbf{K}] +0.27\cos[\mathbf{R}(L^2)\mathbf{K}]+0.13\cos[\mathbf{R}(L^3)\mathbf{K}] ,$$

$$f_{2xx}(\mathbf{K})=0.261 ,$$

$$f_{3xx}(\mathbf{K})=-1.09 ,$$

$$d_{1xx}(\mathbf{K})=7.41-5.75\cos[\mathbf{R}(L^1)\mathbf{K}] -1.49\cos[\mathbf{R}(L^2)\mathbf{K}]-0.17\cos[\mathbf{R}(L^3)\mathbf{K}] ,$$

$$d_{2xx}(\mathbf{K})=-1.55+1.63\cos[\mathbf{R}(L^1)\mathbf{K}] +1.01\cos[\mathbf{R}(L^3)\mathbf{K}]-1.09\cos[\mathbf{R}(L^3)\mathbf{K}] .$$

Again we have assumed f_{2xx} and f_{3xx} to be dispersionless. As expected the shear component f_{2xx} is considerably smaller than the normal component f_{2zz}. Similarly f_{3xx} is much more negative than f_{3zz}. This might simply mean that the prismatic stack of the selenium sheets in the layer would be highly unstable (with respect to the close-packed arrangements) if the short-range Ta-Se interaction would not provide the necessary stabilizing forces.

For f_{1xx} and d_{1xx} the dominant term in the dispersion is still the one proportional to $\cos[\mathbf{R}(L^1)\mathbf{K}]$ which is indicative of a "normal" behavior, whereas d_{2xx} shows the anomaly due to the relatively large contribution of the other components. Thus in f_{1xx} and d_{1xx}, as for z polarization, the nearest-neighbor interaction is dominant, whereas in d_{2x} there are longer-range contributions. This fit, despite its simplicity, permits us to conclude that all the anomalous behavior in $2H$-$_a TaSe_2$ comes from the long-range longitudinal interactions in the tantalum plane, which are responsible for the CDW instability, in agreement with recent microscopic calculations.[13] Furthermore the anomalous behavior of the Reyleigh wave, notably the localization at the zone boundary, is also due to a change of interaction in the tantalum sheet at the surface layer. The temperature dependent anomaly of the Rayleigh wave appearing at one-half of the zone around the CDW transition temperature should also be attributed to the same mechanism.

CONCLUSION

In conclusion we have shown that our DLC approach can be used as a flexible tool in analyzing atom scattering data for surface phonons. Here we have not treated the calculation of surface projected total phonon density

(SPTPD), which can be readily evaluated by weighting the eigenvalues with the displacement of the atoms at the surface. This SPTPD can be used not only to calculate the relative intensities in atom-surface inelastic scattering, but also to evaluate inelastic-electron-tunneling probabilities from surfaces and interfaces. Comparison to experimental spectra, although still semiquantitative, may provide, in turn, additional confirmation to atom-scattering information. This procedure has been adopted for the case of GaSe(001).[3]

Finally we point out that the applications here presented are only a qualitative approach to systems which do not strictly display the appropriate symmetry. Nevertheless, we think that our DLC approach can be used with major benefits, mostly in crystals which possess such a complex structure as to discourage direct slab or Green's function calculations.

ACKNOWLEDGMENTS

We gratefully acknowledge the contribution of Professor G. Benedek for helpful discussions about the application of the DLC method. We are also indebted to Professor J. P. Toennies and to Professor J. G. Skofronick for providing the experimental atom scattering data and for many fruitful discussion. This work was supported in part by NATO Grant. SAS-205-RG(571/83) 463/83 TT and also by the European Economic Community under the Contract No. ST2P-0013-1-F(CD). The authors also belong to the Unità di Milano (L.M.) and Unità di Pavia (L.C.) of the Unità Gruppo Nazionale di Struttura della Materia, Consiglio Nazionale delle Ricerche (Italy), and to the Unità di Milano of Centro Interuniversitario di Struttura della Materia, Ministero della Pubblica Istruzione.

APPENDIX A

If short-range behavior of $\phi_{\alpha\beta}(\mathbf{L} \mid l_3 l_3', ss')$ is assumed, we can define a set $\{S\}$ of values for $\mathbf{L}$ where the ϕ's will be nonvanishing. Therefore the RI condition will be

$$
\begin{aligned}
0 &= \sum_{\mathbf{L}', l_3', s'}^{\{S\}} [\phi_{\alpha\beta}(\mathbf{L}' \mid l_3 l_3', ss') r_\gamma(\mathbf{L}' \mid l_3' s') - \phi_{\alpha\gamma}(\mathbf{L}' \mid l_3 l_3', ss') r_\beta(\mathbf{L}' \mid l_3' s')] \\
&= \sum_{l_3', s'} \sum_{\mathbf{L}}^{\{S\}} \sum_{\mathbf{L}'}^{\{S\}} [\phi_{\alpha\beta}(\mathbf{L}' \mid l_3 l_3', ss') r_\gamma(\mathbf{L} \mid l_3' s') - \phi_{\alpha\beta}(\mathbf{L}' \mid l_3 l_3', ss') r_\beta(\mathbf{L} \mid l_3' s')] \sum_{\mathbf{K}} \frac{1}{N^2} e^{i\mathbf{K}\cdot[\mathbf{R}(\mathbf{L}') - \mathbf{R}(\mathbf{L})]} \\
&= \sum_{\mathbf{K}} \sum_{l_3', s'} \frac{1}{N^2} \left[\phi_{\alpha\beta}(\mathbf{K} \mid l_3 l_3', ss') \left[\sum_{\mathbf{L}}^{\{\tilde{S}\}} [L_\gamma + x_\gamma(l_3' s')] e^{-i\mathbf{K}\cdot\mathbf{R}(\mathbf{L})} \right] \right. \\
&\quad \left. - \phi_{\alpha\gamma}(\mathbf{K} \mid l_3 l_3', ss') \left[\sum_{\mathbf{L}}^{\{\tilde{S}\}} [L_\beta + x_\beta(L_3' k')] e^{-i\mathbf{K}\cdot\mathbf{R}(\mathbf{L})} \right] \right], \quad \{\tilde{S}\} \subset \{S\}
\end{aligned} \tag{A1}
$$

where L_γ and L_β are different from zero only if $\alpha, \beta \in (x, y)$. We consider now $\mathbf{K}$ as a continuous variable and we transform the summation on $\mathbf{K}$ into a two-dimensional integral:

$$
\begin{aligned}
\int \int dK_x dK_y \sum_{l_3', s'} \left[\phi_{\alpha\beta}(\mathbf{K} \mid l_3 l_3', ss') \left[i \frac{\partial}{\partial K_\gamma} + x_\gamma(l_3' s') \right] \sum_{\mathbf{L}}^{\{\tilde{S}\}} e^{-i\mathbf{K}\cdot\mathbf{R}(\mathbf{L})} \right. \\
\left. - \phi_{\alpha\gamma}(\mathbf{K} \mid l_3 l_3', ss') \left[i \frac{\partial}{\partial K_\beta} + x_\beta(l_3' s') \right] \sum_{\mathbf{L}}^{\{\tilde{S}\}} e^{-i\mathbf{K}\cdot\mathbf{R}(\mathbf{L})} \right] .
\end{aligned} \tag{A2}
$$

Taking account that

$$
\begin{aligned}
\int \int \phi_{\alpha\beta}(\mathbf{K} \mid l_3 l_3', ss') \frac{\partial}{\partial K_y} (e^{-i\mathbf{K}\cdot\mathbf{R}(\mathbf{L})}) dK_x dK_y &= \int dK_x e^{-iK_x R_x(\mathbf{L})} [\phi_{\alpha\beta}(\mathbf{K} \mid l_3 l_3', ss') e^{-iK_y R_y(\mathbf{L})} \mid_{K_y = a}^{K_y = b}] \\
&\quad - \int \int dK_x dK_y \left[\frac{\partial}{\partial K_y} \phi_{\alpha\beta}(\mathbf{K} \mid l_3 l_3', ss') \right] e^{-i\mathbf{K}\cdot\mathbf{R}(\mathbf{L})} ,
\end{aligned} \tag{A3}
$$

where a and b are the extreme values of K_y at the SBZ for a given K_x. The first term in the right side of Eq. (A3) vanishes for symmetry reasons, so that extending this relation to $K_\gamma = K_x$ or K_y and $K_\beta = K_x$ or K_y in (A2) we obtain, getting back to a discrete $\mathbf{K}$ space,

$$\sum_{\mathbf{K}} \sum_{\mathbf{L}}^{\{\tilde{S}\}} \frac{1}{N^2} \left\{ \sum_{l_3',s'} [\phi_{\alpha\beta}(\mathbf{K} \mid l_3 l_3', ss') x_\gamma(l_3' s') - \phi_{\alpha\beta}(\mathbf{K} \mid l_3 l_3', ss') x_\beta(l_3' s')] \right.$$
$$\left. -i \left[\frac{\partial}{\partial K_\gamma} \left[\sum_{l_3',s'} \phi_{\alpha\beta}(\mathbf{K} \mid l_3 l_3', ss') \right] - \frac{\partial}{\partial K_\beta} [\phi_{\alpha\beta}(\mathbf{K} \mid l_3 l_3', ss')] \right] \right\} e^{-i\mathbf{K}\cdot\mathbf{R}(\mathbf{L})} = 0 \ . \quad \text{(A4)}$$

Now because of the arbitrariness of the set $\{\tilde{S}\}$, which was supposed to be only larger than $\{S\}$, the double summation of expression (A4) is zero only if each term of the sum is zero and we obtain

$$\sum_{l_3',s} [\phi_{\alpha\beta}(\mathbf{K} \mid l_3 l_3', ss') x_\gamma(l_3' s') - \phi_{\alpha\gamma}(\mathbf{K} \mid l_3 l_3', ss') x_\beta(l_3' s')] = i \left[\frac{\partial}{\partial K_\gamma} d_{\alpha\beta}(\mathbf{K} \mid l_3 s) - \frac{\partial}{\partial K_\beta} d_{\alpha\gamma}(\mathbf{K} \mid l_3 s) \right] \quad \text{(A5)}$$

where we have used definition (7a). Equation (A5) differs from a strictly linear-chain RI condition on the right side, which is not zero. In some cases it is quite small and can be ignored in a first-order approximation. At least, $d_{\alpha\alpha}(\mathbf{K} \mid l_3 s)$, which is the leading term, is known by the fitting procedure.

If the surface-phonon analysis require xz coupling, and mixed force constants are obtained via RI condition or by *ad hoc* perturbation [as in the case of GaSe(001)], we can take into account *a posteriori* this coupling by solving the eigenvalue problem for

$$\begin{bmatrix} \omega_x^2 & e_x^* D_{xz} e_z \\ e_z^* D_{zx} e_x & \omega_z^2 \end{bmatrix} \begin{bmatrix} W_x \\ W_z \end{bmatrix} = \tilde{\omega}^2 \begin{bmatrix} W_x \\ W_z \end{bmatrix} , \quad \text{(A6)}$$

where ω_x^2 and ω_z^2 are the diagonal matrices of eigenvalues for the uncoupled system, D_{xz} and D_{zx} are the blocks of mass-scaled mixed force constants. The eigenvectors of the coupled problem are obtained by

$$\begin{bmatrix} E_x \\ E_z \end{bmatrix} = \begin{bmatrix} e_z & 0 \\ 0 & e_z \end{bmatrix} \begin{bmatrix} W_x \\ W_z \end{bmatrix} , \quad \text{(A7)}$$

where e_x and e_z are the matrices formed by all the eigenvectors of the uncoupled system and E_x, E_y are column eigenvectors of Eq. (A6) for a particular $\mathbf{K}$.

APPENDIX B

We give the surface lattice points (in units of a). For the first shell,

$$\mathbf{L}^0 = (0,0) ,$$
$$\mathbf{L}^1 = (\sqrt{3/2}, 1/2), \quad \mathbf{L}^4 = -\mathbf{L}^1 ,$$
$$\mathbf{L}^2 = (0,1), \quad \mathbf{L}^5 = -\mathbf{L}^2 ,$$
$$\mathbf{L}^3 = (-\sqrt{3/2}, 1/2), \quad \mathbf{L}^6 = -\mathbf{L}^3 .$$

For the second shell,

$$\mathbf{L}^7 = (\sqrt{3}, 0), \quad \mathbf{L}^{10} = -\mathbf{L}^7 ,$$
$$\mathbf{L}^8 = (\sqrt{3/2}, 3/2), \quad \mathbf{L}^{11} = -\mathbf{L}^8 ,$$
$$\mathbf{L}^9 = (-\sqrt{3/2}, 3/2), \quad \mathbf{L}^{12} = -\mathbf{L}^9 .$$

For the third shell,

$$\mathbf{L}^{13} = (\sqrt{3}, 1), \quad \mathbf{L}^{16} = -\mathbf{L}^{13} ,$$
$$\mathbf{L}^{14} = (0,2), \quad \mathbf{L}^{17} = -\mathbf{L}^{14} ,$$
$$\mathbf{L}^{15} = (-\sqrt{3}, 1), \quad \mathbf{L}^{18} = -\mathbf{L}^{15} .$$

For the fourth shell,

$$\mathbf{L}^{19} = (3\sqrt{3/2}, 1/2), \quad \mathbf{L}^{25} = -\mathbf{L}^{19} ,$$
$$\mathbf{L}^{20} = (\sqrt{3}, 2), \quad \mathbf{L}^{26} = -\mathbf{L}^{20} ,$$
$$\mathbf{L}^{21} = (\sqrt{3/2}, 5/2), \quad \mathbf{L}^{27} = -\mathbf{L}^{21} ,$$
$$\mathbf{L}^{22} = (-\sqrt{3/2}, 5/2), \quad \mathbf{L}^{28} = -\mathbf{L}^{22} ,$$
$$\mathbf{L}^{23} = (\sqrt{3}, 2), \quad \mathbf{L}^{29} = -\mathbf{L}^{23} ,$$
$$\mathbf{L}^{24} = (-3\sqrt{3/2}, 1/2), \quad \mathbf{L}^{30} = -\mathbf{L}^{24} .$$

APPENDIX C

If we label $\phi_{\alpha\beta}(\mathbf{L}^n \mid l_3 l_3', ss')$ by $\phi(n)$, where $\mathbf{L}^n$ refers to the points in Appendix B, Eq. (1) can be expanded as follows:

$$\phi(\bar{\mathbf{K}}) = \sum_{n=1}^{30} \phi(n) e^{i\bar{\mathbf{K}}\cdot\mathbf{R}(\mathbf{L}^n)}$$
$$= \phi(0) + [\phi(1) + \phi(4)] \cos\left[\bar{K}_n \frac{\sqrt{3}}{2} a + \bar{K}_y \frac{1}{2} a \right] + [\phi(2) + \phi(5)] \cos(\bar{K}_y a) + [\phi(3) + \phi(6)] \cos\left[-\bar{K}_x \frac{\sqrt{3}}{2} a + \bar{K}_y \frac{1}{2} a \right]$$

$$+[\phi(7)+\phi(10)]\cos(\bar{K}_x\sqrt{3}a)+[\phi(8)+\phi(11)]\cos\left[\bar{K}_x\frac{\sqrt{3}}{2}a\bar{K}_y\frac{3}{2}a\right]$$

$$+[\phi(9)+\phi(12)]\cos\left[-\bar{K}_x\frac{\sqrt{3}}{2}a+\bar{K}_y\frac{3}{2}a\right]+[\phi(13)+\phi(16)]\cos(\bar{K}_x\sqrt{3}a+\bar{K}_y a)$$

$$+[\phi(14)+\phi(17)]\cos(\bar{K}_y 2a)+[\phi(15)+\phi(18)]\cos(-\bar{K}_x\sqrt{3}a+\bar{K}_y a)$$

$$+[\phi(19)+\phi(25)]\cos\left[\bar{K}_x\frac{3}{2}\sqrt{3}a+\bar{K}_y\frac{1}{2}a\right]+[\phi(20)+\phi(26)]\cos(\bar{K}_x\sqrt{3}a\bar{K}_y 2a)$$

$$+[\phi(21)+\phi(27)]\cos\left[\bar{K}_x\frac{\sqrt{3}}{2}a+\bar{K}_y\frac{5}{2}a\right]+[\phi(22)+\phi(28)]\cos\left[-\bar{K}_x\frac{\sqrt{3}}{2}a+\bar{K}_y\frac{5}{2}a\right]$$

$$+[\phi(23)+\phi(29)]\cos(-\bar{K}_x\sqrt{3}a+\bar{K}_y 2a)+[\phi(24)+\phi(30)]\cos\left[-\bar{K}_x\frac{3}{2}\sqrt{3}\alpha+\bar{K}_y\frac{a}{2}\right]. \tag{C1}$$

However if $\bar{\mathbf{K}}$ is taken with only an x or y component, as is possible by exploiting the SBZ symmetry, Eq. (C1) can be regrouped and generalized:

$$\begin{aligned}\phi(\bar{\mathbf{K}})=&\phi(0)+[\phi(1)+\phi(4)+\phi(3)+\phi(6)]\cos[\bar{K}_\beta R_\beta(L^1)]+[\phi(2)+\phi(5)]\cos(\bar{K}_\beta L_\beta^2)\\&+[\phi(7)+\phi(10)]\cos[\bar{K}_\beta R_\beta(L^7)]+[\phi(8)+\phi(11)+\phi(9)+\phi(12)]\cos[\bar{K}_\beta R_\beta(L^8)]\\&+[\phi(13)+\phi(16)]\cos(\bar{K}_\beta L_\beta^{13})+[\phi(14)+\phi(17)]\cos[\bar{K}_\beta R_\beta(L^{14})]+[\phi(15)+\phi(18)]\cos[\bar{K}_\beta R_\beta(L^{15})]\\&+[\phi(19)+\phi(25)+\phi(24)+\phi(30)]\cos[\bar{K}_\beta(L^{19})]+[\phi(20)+\phi(26)+\phi(23)+\phi(29)]\cos[\bar{K}_\beta R_\beta(L^{20})]\\&+[\phi(21)+\phi(27)+\phi(22)+\phi(28)]\cos[\bar{K}_\beta R_\beta(L^{21})],\end{aligned} \tag{C2}$$

where $\beta=x$ or y. It is clear that each coefficient in the cosine expansion takes account of several $\phi(n)$. The relative weight of these terms depends on the crystal geometry and on the range of the force constant which is expanded. In the case of GaSe we have selected for $\bar{\mathbf{K}}$ the values at the $\bar{\Gamma}$, Σ, $\bar{M}$, $\bar{K}$, and T' points of the SBZ (see Fig. 3) and we have restricted our fitting to the second shell of $\mathbf{L}^n$:

$$\begin{aligned}\phi(\bar{\mathbf{K}})=&\phi(0)+[\phi(1)+\phi(4)+\phi(3)+\phi(6)]\cos[\bar{K}_\beta R_\beta(L^1)]+[\phi(2)+\phi(5)]\cos[\bar{K}_\beta R_\beta(L^2)]\\&+[\phi(7)+\phi(10)]\cos[\bar{K}_\beta R_\beta(L^7)]+[\phi(8)+\phi(11)+\phi(9)+\phi(12)]\cos[\bar{K}_\beta R_\beta(L^8)].\end{aligned} \tag{C3}$$

Thus the expansion coefficients are found by solving the linear system in the unknown variables [groups of $\phi(n)$] enclosed in square brackets of Eq. (C3).

For the case of $TaSe_2$ we have made the fitting only along the x direction by selecting for $\bar{\mathbf{K}}$ the values at the $\bar{\Gamma}$, $\bar{M}$, Σ', and Σ'' points of the SBZ (see Fig. 3) and by regrouping Eq. (C2) up to the 30th term (see Appendix B) as follows:

$$\begin{aligned}\phi(\bar{K}_x)=&[\phi(0)+\phi(2)+\phi(5)+\phi(14)+\phi(17)]+[\phi(1)+\phi(3)+\phi(4)+\phi(6)+\phi(8)+\phi(9)+\phi(11)\\&+\phi(12)+\phi(21)+\phi(22)+\phi(27)+\phi(28)]\cos[\bar{K}_x(\sqrt{3}/2)a]\\&+[\phi(7)+\phi(10)+\phi(13)+\phi(15)+\phi(16)+\phi(18)+\phi(20)+\phi(23)+\phi(26)+\phi(29)]\cos(\bar{K}_x\sqrt{3}a)\\&+[\phi(19)+\phi(24)+\phi(25)+\phi(30)]\cos(\bar{K}_x\tfrac{3}{2}\sqrt{3}a).\end{aligned} \tag{C4}$$

Solutions of the 4×4 linear system are obtained in the same way as the GaSe case.

Special consideration is given to $d_{\alpha\beta}$ which, according to expression (8) has to be fitted with a separate procedure:

$$d_{\alpha\beta}(\bar{\mathbf{k}}\mid l_3 s)=\sum_{\substack{l_3',s'\\(l_3's')\neq(l_3s)}}[\phi_{\alpha\beta}(\bar{\mathbf{K}}\mid l_3 l_3',ss')-\phi_{\alpha\beta}(\mathbf{K}=\mathbf{0}\mid l_3 l_3',ss')]+\sum_{\mathbf{L}(\neq\mathbf{0})}\phi_{\alpha\beta}(\mathbf{L}\mid l_3 l_3,ss)(e^{i\bar{\mathbf{K}}\cdot\mathbf{R}(\mathbf{L})}-1), \tag{C5}$$

so that the second term in the right side can be fitted as long as the first term has been subtracted from the value of $d_{\alpha\beta}(\bar{\mathbf{K}}\mid l_3 s)$. This procedure will give us straight forwardly the in-plane force constants of the crystal, $\bar{d}_{s\alpha\alpha}(\mathbf{L})=\phi_{\alpha\alpha}(\mathbf{L}\mid l_3 l_3,ss)$.

[1]G. Brusdeylins, R. Rechsteiner, J. G. Skofronick, J. P. Toennies, G. Benedek, and L. Miglio, Phys. Rev. B **34**, 902 (1986).

[2]G. Benedek, G. Brusdeylins, C. Heimlich, L. Miglio, J. G. Skofronick, and J. P. Toennies, J. Vac. Sci. Technol. A **5**, 1093 (1987); Europhys. Lett. (to be published).

[3]L. Miglio and G. Benedek, Europhys. Lett. **3**, 619 (1987).

[4]F. W. de Wette and G. P. Alldredge, in *Methods in Computational Physics,* edited by G. Gilet (Academic, New York, 1976), Vol. 15, p. 163.

[5]*Electrons and Phonons in Layered Crystal Structure,* edited by J. J. Wieting and M. Schlüter (Reidel, Dordrecht, 1979); F. Hulliger, *Structural Chemestry of Layer-type Phases* (Reidel, Dorderecht, 1976).

[6]J. L. Feldman, Phys. Rev. B **25**, 7132 (1982).

[7]S. Jandl, J. L. Brebner, B. M. Powell, Phys. Rev. B **13**, 686 (1976).

[8]D. E. Moncton, J. D. Axe, and F. J. Di Salvo, Phys. Rev. Lett. **34**, 734 (1975); Phys. Rev. B **16**, 801 (1977).

[9]L. Miglio and G. Benedek, in *Topics in Current Physics,* edited by W. Schommers and P. Van Blanchenhagen (Springer, Berlin, 1987), Vol. 43.

[10]M. Posternak, A. Baldereschi, A. J. Freeman, and E. Winner, Phys. Rev. Lett. **52**, 863 (1984).

[11]M. Schluter, J. Camassel, S. Kohn, J. P. Voitchousky, Y. R. Shen, and M. L. Cohen, Phys. Rev. B **13**, 2524 (1967).

[12]J. A. Holy, M. V. Klein, W. L. McMillan, and S. F. Meyer, Phys. Rev. Lett. **37**, 1145 (1976); J. C. Tsang, J. E. Smith, Jr., and M. W. Shafer, Solid State Commun. **27**, 145 (1978).

[13]K. Motizuki, K. Kimura, E. Ando, and N. Suzuki, J. Phys. Soc. Jpn. **53**, 1078 (1984).

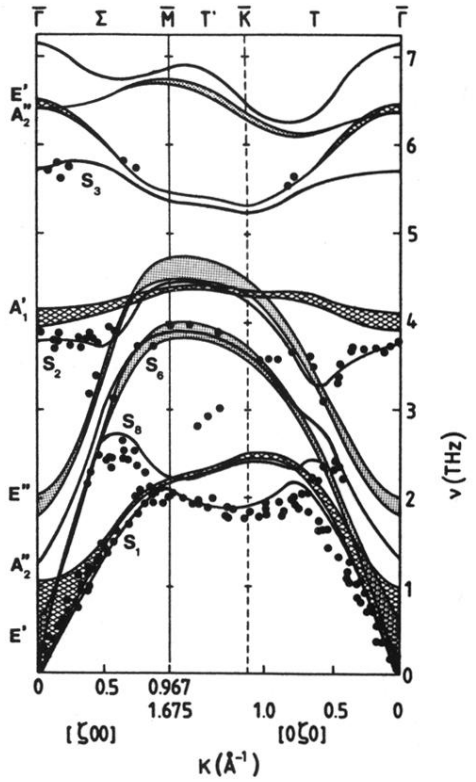

FIG. 5. Dispersion relations for bulk (shaded areas) and surface (solid lines) modes of ϵ-GaSe calculated along the borders of the Surface Brillouin Zone. Solid circles are experimental atom-scattering data from Ref. 1.

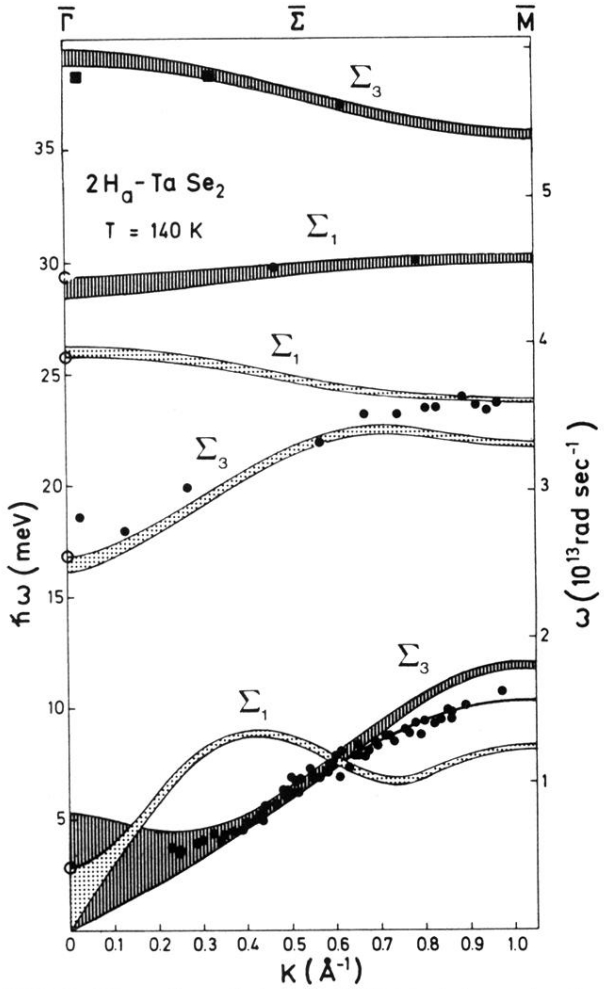

FIG. 6. Dispersion relations for bulk (shaded areas) and surface (solid line) modes of $2H_a$-$TaSe_2$, calculated along the $\overline{\Gamma}\,\overline{M}$ direction. Dotted bands display nearly-x polarization and the other ones have nearly-z displacements. Solid circles ($T=140$ K) and solid squares ($T=60$ K) represent experimental atom-scattering data from Ref. 2.